ChemPubSoc Europe
DOI: 10.1002/cctc.201701194
CHEMCATCHEM Full Papers

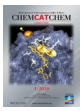

Switching the Cofactor Specificity of an Imine Reductase

Niels Borlinghaus and Bettina M. Nestl*[a]

In the last years, imine reductases (IREDs) have gained importance for the formation of chiral amines by catalyzing asymmetric reductions of imines and chemo- and stereoselective reductive aminations. However, all characterized members of this steadily growing enzyme family demonstrated strict preference for NADPH, which entails reduced possibilities for efficient cofactor regenerations and limitations in the construction of whole cell systems. To alter the cofactor specificity from NADPH to NADH, we applied the "Cofactor Specificity Reversal—Structural Analysis and Library Design" (CSR-SALAD) mutagenesis strategy and enlarged the mutant library by further amino acid replacements. This engineering approach has been shown to result in IRED variants with up to 2900-fold improved NADH/NADPH specificity and completely recovered activity in the reduction of 2-methyl pyrroline (2MP).

Introduction

Chiral amines are powerful building blocks of high significance, which are used for the synthesis of a variety of industrially relevant chemicals.[1] Over the last few years, different methodologies have been developed for their synthesis. In this light, transaminases,[2] lipases,[3] ammonia lyases,[4] amine dehydrogenases,[5] monoamine oxidases,[6] and imine reductases (IRED)[7] are efficient biocatalysts for preparing chiral amines in high stereoselectivity. Although the majority of these enzymes generate only primary amines, IREDs can catalyze imine reductions and reductive aminations with direct access also to secondary and tertiary amines featuring excellent enantiopurity (Scheme 1).[7–10] A broad range of amines was produced by using IREDs that were applied as isolated enzymes, in multienzyme cascades, and whole cell approaches.[11–14]

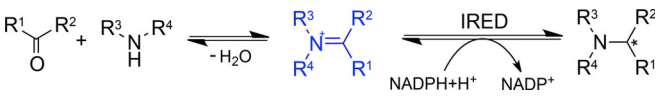

Scheme 1. General scheme of IRED-catalyzed reactions. Imines and iminium ions are reduced by IRED by using NADPH as cofactor to afford amines. The imine substrate (shown in blue) can be directly reduced or formed through reaction of a carbonyl group with an amine.

To enable economic biotransformations on the industrial scale, in situ cofactor regeneration of the expensive nicotinamide cofactor is required. Thus, only a catalytic amount of NAD(P)H is needed and the cost can be notably reduced. Furthermore, cofactor regeneration can drive the reaction to completion and allow the removal of oxidized cofactor. The development of various NAD(P)H cofactor regeneration processes has been subject to intensive studies.[15–20] In most regeneration schemes for nicotinamide cofactors, the desired enzymatic reduction step is coupled to another enzymatic reaction. Several enzymatic methods have been described, such as the reduction of NAD^+ with the formate dehydrogenase (FDH) from *Candida boidini*,[21,22] the phosphite dehydrogenase (PTDH) from *Pseudomonas stutzeri*,[23] or the soluble hydrogenase from *Ralstonia eutropha* H16.[24] These systems distinguish themselves because they are cost-saving substrates, have excellent atom efficiency, and do not hinder the product workup after reaction.[25]

In contrast to the regeneration of NADH, the accessibility of NADPH regenerating enzymes is rare and the available systems show quite low applicability.[15] Different approaches were proposed to overcome these limitations, including engineered formate dehydrogenase and phosphite dehydrogenase variants with switched cofactor specificity[27–31] and whole cell systems using the natural cofactor regeneration by cellular metabolism. However, the allocation of NADPH is limited to about 0.1 U mg^{-1} cell dry weight, and might be not sufficient for enzymes with high activity.[15] Furthermore, there have been many reported successes of enzyme redesign for altered cofactor specificity utilizing directed evolution, site-directed mutagenesis, or (semi)-random saturation mutagenesis.[32,33]

Recently, the group of Höhne reported the generation of an IRED variant by rational design demonstrating a three-fold increased activity for NADH with 10% activity recovery.[34] To address this important challenge of improving the specificity and activity for NADH, we altered the cofactor specificity of the *R*-selective IRED from *Myxococcus stipitatus* (*R*-IRED_*Ms*) by using the recently described online tool "Cofactor Specificity Reversal—Structural Analysis and Library Design" (CSR-SALAD), developed in the lab of Frances H. Arnold. CSR-SALAD is a semi-rational structure-guided approach that aims at reversing the nicotinamide cofactor specificity of enzymes with Rossman

[a] *N. Borlinghaus, Dr. B. M. Nestl*
Institute of Biochemistry and Technical Biochemistry, Chair of Technical Biochemistry
University of Stuttgart
Allmandring 31, 70569 Stuttgart (Germany)
E-mail: bettina.nestl@itb.uni-stuttgart.de

Supporting information for this article can be found under: https://doi.org/10.1002/cctc.201701194.

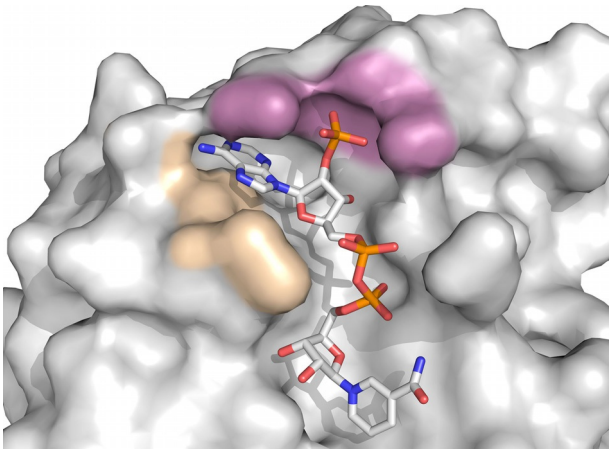

Figure 1. Rossman fold NADPH binding pocket of (*R*)-selective IRED from *Myxococcus stipitatus*. Specificity determining regions are shown in magenta (2′-phosphate coordinating) and light orange (not 2′-phosphate coordinating). The 3D model was generated by using the SWISS-MODEL server (template PDB code 3ZHB[26]).

fold binding pockets as in the case of IREDs (Figure 1).[35] This approach includes the simultaneous mutagenesis of phosphate coordinating residues, which generally determine the cofactor specificity. Compared with a combined saturation mutagenesis, the suggested mutant library is strongly reduced and, thus, does not require high throughput screening. Furthermore, CSR-SALAD predicts additional positions in the cofactor binding pocket to recover the activity subsequently with a handful of site-saturation mutagenesis approaches. This promising tool and the first insights from the group of Höhne inspired us to switch the cofactor specificity of *R*-IRED_*Ms* while ensuring recovery of the enzymatic activity. Herein, we report the stepwise mutagenesis in the cofactor binding pocket of *R*-IRED_*Ms* by utilizing CSR-SALAD.

Results and Discussion

Owing to the fact that the crystal structure of *R*-IRED *Ms* has not been determined yet, we used the structure of the closely related *R*-selective IRED from *Streptomyces kanamyceticus* (*R*-IRED_*Sk*, PDB code 3ZHB, 42% identity, Supporting Information Figure S1) for CSR-SALAD analysis. Cahn et al. demonstrated in previous work the robustness of CSR-SALAD including one protein without a crystal structure.[35] Recommended mutations for *R*-IRED_*Sk* at seven positions were transferred onto *R*-IRED_*Ms*. Four positions were located around the 2′-phosphate moiety of NADPH and the other amino acids were positioned opposite to the phosphate binding pocket (Figure 2).

We generated the first mutant library by changing three of the four phosphate coordinating residues (R33, T34, K37) simultaneously against the suggested amino acids. We used three degenerated codons (HVC, RMK, and DMK) coding for different numbers of amino acids, resulting in a reduced mutant library of 432 members (Table S2 in the Supporting Information). For the screening of the mutant library, we developed a deep-well plate-based NAD(P)H consumption assay.

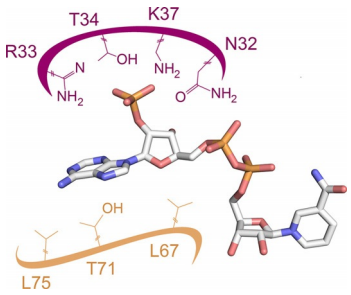

Figure 2. Selected target residues of *R*-IRED_*Ms* for switching the cofactor specificity. Residues in the phosphate coordinating pocket are highlighted in magenta. Further residues are shown in light orange.

The decrease in absorbance at 340 nm was monitored in the conversion of 2-methylpyrroline (2MP) to 2-methylpyrrolidine (2MPD) by using cell-free lysates. In the first round of mutagenesis, we were able to identify four variants with improved specificity. Interestingly, all of them carry a tyrosine at position 33, followed by polar (N, T) or even charged residues (D, E, K) at positions 34 and 37 (Figure S2 in the Supporting Information). Best results were obtained by the double variant R33Y/T34E (**V1**) with no substitution at position K37. The necessity of the combined modifications was tested by generating the R33Y single mutant, which showed 21-fold lower specificity than **V1** (Figure S5 in the Supporting Information).

To test whether additional substitutions at position 37 could contribute to the properties of the double variant, we supplemented the library, performing a site-saturation mutagenesis by using **V1** as a template. The substitution of lysine by alanine or arginine had a marked effect on either the specificity (YEA, **V2**) or activity (YER, **V3**). The data are given in Figure 3 and Figure S3 (in the Supporting Information).

Both variants were used as templates for the site-saturation mutagenesis at position 32, which was predicted by CSR-SALAD to mainly influence the activity. Although no increase in activity could be observed, remarkable improvements in specificity were noticed by introducing the variant N32E (**V4** and

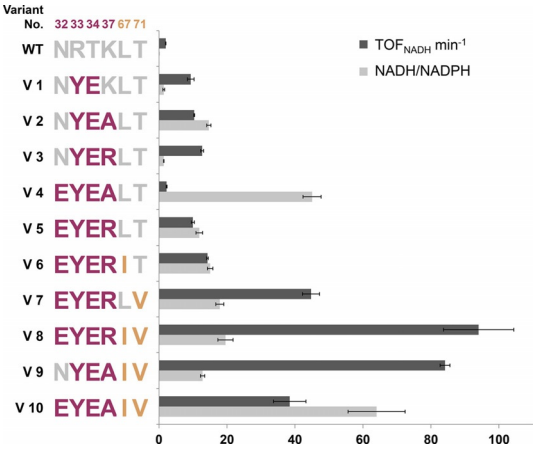

Figure 3. Turnover frequencies with NADH (dark gray) and NADH/NADPH specificities (gray) of generated *R*-IRED_*Ms* variants compared with the wild-type enzyme (WT).

V5). Variant **V4** demonstrated the highest specificity; however, the overall activity was distinctly reduced. After three rounds of mutagenesis and screening, we were able to identify two promising variants (**V2** and **V5**) with about five times increased activities and over 500-fold improved specificities towards NADH. Further, we performed site-saturation mutagenesis at positions 67, 71, and 75. We thus focused our engineering on **V5** and subsequently transferred the most promising substitutions to **V2**. Saturating position L75 did not lead to improved variants. In contrast to L75, improved variants were obtained by saturating positions L67 and T71. Substituting L67 with isoleucine led to a slightly increased specificity and activity (**V6**). Through mutagenesis of T71, three variants with remarkable improvements were identified. Interestingly, all of them showed hydrophobic replacements (Figure S4 in the Supporting Information), with T71V featuring the highest activity (**V7**). We then combined L67I and T71V (**V8**) and observed strong synergistic effects, reaching a 47-fold increased NADH activity and a 900-times improved specificity compared with the wild-type (Figure 3, Table 2). Remarkably, we achieved a completely recovered activity with a turnover frequency (TOF) of 94 min^{-1} comparable to the wild-type with 91 min^{-1}. Similar observations were made when we transferred L67I and T71V to variant 2 (**V9**), resulting in a TOF of 84 min^{-1}. To further increase the specificity of **V9**, we introduced mutation N32E (**V10**). This variant showed a 2900-times improved specificity compared with the wild-type. However, a reduction of activity with NADH was detected (TOF = 38 min^{-1}).

The kinetic parameters of **V8** and **V10** were determined to further validate the influence of these mutations in the asymmetric reduction of 2-MP by using NADPH and NADH as cofactors (Table 1 and Figure S6 in the Supporting Information). Confirming the observed activities and specificities, both variants showed improved catalytic efficiencies if NADH was used. The k_{cat} value of **V8** with NADH was even 1.7-fold higher compared with the wild-type with its natural cofactor.

Next, we performed biotransformations by using 2-MP as the substrate to evaluate product formations and selectivities (Table 2). Biocatalytic reactions were stopped after 45 min, shortly before the wild-type enzyme reached full conversion with NADPH. At the same time, the tested variants formed only 46% (**V8**) and 11% (**V10**) of product (2MPD) if NADPH was used. The opposite development was noticed if NADH was applied. In contrast to the wild-type (14% product formation), variants **V8** and **V10** showed excellent conversions of >98% and 94%, respectively. Remarkably, the high enantioselectivity of the wild-type enzyme with >98% *ee* (*R*) was unchanged for both variants.

For a better understanding of the structural changes in the cofactor binding pocket of **V8** and **V10**, we calculated possible arrangements in silico with YASARA.[36] We ran 0.5 ns molecular dynamics (MD) refinements by using energy-minimized homology models as the starting structures. The comparison of the resulting structures enabled us to presume how individual residues influence the cofactor stability (Figure 4). The most influential mutation R33Y is found in all initial variants. One important impact of this mutation might be the destabilization of NADPH, as the positively charged arginine is described to be the favored interaction partner of the negatively charged 2′-phosphate.[35] However, this only occurs when further phosphate coordinating residues in positions 32, 34, and 37 were replaced. In this context, the introduction of glutamic acid at positions 32 or 34 might cause a reduced acceptance of NADPH by electrostatic repulsion.

Position 37 seems to be also involved in the stabilization of NADH and the residue at this position is the only discriminator between variants **V8** and **V10**. We assumed that arginine at this position (**V8**) is able to stabilize NADH better than alanine (**V10**). However, K37R should reduce the repulsion of NADPH owing to its positive charge. This might explain why variants with K37R show a lower specificity for NADH than variants with other mutations at this position, such as K37A, K37M, or K37Q (Figure S3 in the Supporting Information).

Table 1. Kinetic parameters of variants **8** and **10** compared with the wild-type (WT) enzyme by using 2-methylpyrroline (2MP) as the substrate.

	NADPH				NADH			
	K_M [mM]	k_{cat} [s^{-1}]	K_I [mM]	k_{cat}/K_M [min^{-1}/mM^{-1}]	K_M [mM]	k_{cat} [s^{-1}]	K_I [mM]	k_{cat}/K_M [min^{-1}/mM^{-1}]
WT	1.0 ± 0.1	2.3 ± 0.1	20 ± 2	134 ± 16	23 ± 1	0.09 ± 0.003	12 ± 1	0.2 ± 0.01
V8	12 ± 2	0.14 ± 0.01	11 ± 2	0.7 ± 0.1	9.8 ± 0.3	3.9 ± 0.04	21 ± 0.2	24 ± 1
V10	6.8 ± 0.9	0.02 ± 0.002	16 ± 4	0.2 ± 0.03	11 ± 2	1.5 ± 0.2	29 ± 6	7.9 ± 1.6

Table 2. Activities and specificities of variants **8** and **10** compared with the wild-type enzyme by using 2-methylpyrroline (2MP) as the substrate.

	NADPH			NADH			Specificity	
	TON[a] [min^{-1}]	Conversion[b] [%]	*ee*[b] [%]	TON[a] [min^{-1}]	Conversion[b] [%]	*ee*[b] [%]	NADH/NADPH[a] [min^{-1}/min^{-1}]	Fold change from wild-type
WT	91 ± 2	>98	>98 (*R*)	2.0 ± 0.07	14 ± 1.7	>98 (*R*)	0.022 ± 0.001	–
V8	4.8 ± 0.2	46 ± 2	>98 (*R*)	94 ± 10	>98	>98 (*R*)	20 ± 2	900 ± 100
V10	0.6 ± 0.02	11 ± 1	>98 (*R*)	38 ± 5	94 ± 3	>98 (*R*)	64 ± 8	2900 ± 400

[a] 10 mM 2-methylpyrroline, 0.4 mM NAD(P)H, pH 7.0, 25 °C. [b] 8 mM 2-methylpyrroline, 10 mM NAD(P)H, 2 μM enzyme, 45 min, 25 °C, 180 rpm.

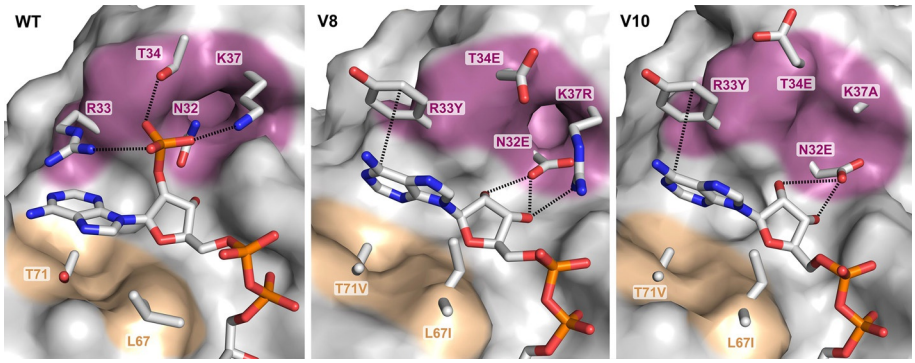

Figure 4. 3D model of the wild-type NADPH binding pocket in *R*-IRED_*Ms* (WT) and the cofactor binding pockets of **V8** and **V10** with bound NADH instead of NADPH. The shown arrangements were calculated with Yasara[36] running 0.5 ns MD refinements by using energy minimized homology models as starting structures. Selected and mutated regions are shown in magenta (2′-phosphate coordinating) and light orange (not 2′-phosphate coordinating). Calculated distances between the 2′-phosphate moiety and residues R33, T34, and K37 (WT) are 2.6–3.0 Å. The distance between the 6′-carbon of adenine and tyrosine at position 33 (**V8**, **V10**) is 4.4 Å. Distances between the 2′- and 3′-hydroxyl groups of NAD(H) and glutamic acid at position 32 (**V8**, **V10**) are 2.6–3.5 Å. The distance between the 3′-hydroxyl group of NAD(H) and arginine at position 37 (**V8**) is 3.0 Å.

Furthermore, we assume that the exact positioning of the cofactor in the binding pocket is essential for the stabilization of NADH. In this regard, R33Y appears to be particularly important as the tyrosine residue allows the rearrangement of the cofactor through stacking interactions to adenine. To allocate the NADH cofactor in a novel binding mode, alterations in the native adenine binding pocket by mutations L67I and T71V were required.

The elimination of a hydrogen bridge through substitution of T71 against valine shall result in a reduced affinity of the cofactor in its native conformation. Consequently, MD refinements in silico verified that the cofactor is slightly rotated and shifted (Figure 4). We hypothesize that this reorientation facilitates the establishment of stronger binding modes so that the induced NADH specificity is accompanied by high activity.

Conclusions

The presented engineering procedure using CSR-SALAD serves as a powerful tool for introducing enzyme specificity towards a non-native cofactor. We identified NADH-dependent IRED variants by altering the cofactor binding pocket of the (*R*)-selective IRED from *Myxococcus stipitatus*. The mutagenesis of the 2′-phosphate binding pocket resulted in considerable improvements regarding the NADH/NADPH specificity. Additional substitutions of L67 and T71 resulted in variants with reversed specificity and recovered activity.

Experimental Section

Cloning, protein expression, and purification

The gene of *R*-IRED_*Ms* was cloned into the pBAD33 plasmid using a Gibson Assembly and fused with an N-terminal his6-tag. For the expression, we used *E. coli* JW5510 cells harboring the vector and let them grow as preculture overnight at 37 °C. Next, we inoculated terrific broth (TB) culture medium containing 34 μg mL^{-1} chloramphenicol with 0.25% preculture. After a 2–3 h incubation at 37 °C and reaching an optical density of OD_{600} = 0.8–1.0, the protein expression was induced with the addition of arabinose (final concentration 0.02%). Then, the cultures were incubated for about 20 h at 25 °C. Cells were harvested and then lysed with a high-pressure homogenizer. Protein purification was performed with cobalt His-Trap columns (His-GraviTrap-TALON, Healthcare) using buffer A (50 mM potassium phosphate buffer pH 7.0, 300 mM KCl) for binding, buffer B (50 mM potassium phosphate buffer pH 7.0, 300 mM KCl, 5 mM imidazole) for washing, and buffer C (50 mM potassium phosphate buffer pH 7.0, 300 mM KCl, 500 mM imidazole) for eluting the enzyme. Afterwards, the buffer was changed by dialysis (two times, 2 h in 5 L, 50 mM potassium phosphate buffer pH 7.0, MWCO = 6–8 kDa). Purity and size was verified by SDS-PAGE (Figure S10 in the Supporting Information). The protein concentration was determined by using the BCA Protein Assay Kit (Thermo Scientific).

Library creation and screening

For the simultaneous exchange of selected amino acids at three positions (R33, T34, K37), degenerated codons (Table S1 in the Supporting Information) suggested by CSR-SALAD were used. We used the primer to integrate the mutations via Gibson assembly. For the site-saturation mutagenesis approaches, we used the QuikChange™ protocol from Stratagene by using a primer with the degenerated NNK codon (N = A, C, G, T; K = T, G) at the corresponding position. Chemical competent *E. coli* JW5510 cells were transformed with the modified DNA (60 s, 42 °C), spread on LB plates (34 μg mL^{-1} chloramphenicol), and grown at 37 °C overnight to obtain between 100 and 400 chloramphenicol-resistant colonies.

For the screening, single colonies were picked to inoculate the preculture by using deep well plates (34 μg mL^{-1} chloramphenicol). After incubation overnight at 25 °C, the preculture was used to inoculate the expression culture (34 μg mL^{-1} chloramphenicol, 0.02% arabinose). The next day, the cells were harvested and stored at −80 °C overnight. Afterwards, the pellets were resuspended in lysis buffer (50 mM potassium phosphate buffer pH 7.0, 750 μg mL^{-1} lysozyme, and 10 μg mL^{-1} DNAse I) and incubated for 1 h at 37 °C. The suspension was centrifuged and the IRED-containing supernatant was used for the NAD(P)H assay (50 mM potassium phosphate buffer pH 7.0, 10 mM 2-methylpyrroline, 0.4 mM NAD(P)H). The NAD(P)H consumption was detected for 30 min at 340 nm in the

plate reader. For the activity calculation, we determined the relation between A_{340} and the NAD(P)H concentration to get the molar attenuation coefficient of $\varepsilon_{NADH} = 3.2632\ A_{340}\,mM^{-1}$ and $\varepsilon_{NADPH} = 3.4069\ A_{340}\,mM^{-1}$.

Enzyme activity assay

For the detection of the enzyme activity, we used defined concentrations of purified enzyme (0.2–20 μM) and incubated them together with 10 mM 2-methylpyrroline and 0.4 mM NAD(P)H in the plate reader at room temperature. The cofactor consumption was measured for 30 min at 340 nm. For kinetic studies, we used the same protocol with varying concentrations of the substrate.

Biotransformation and sample preparation for the GC

Biotransformations of 2-methylpyrroline were performed in glass vials with 2 μM of purified enzyme, 8 mM of 2-methylpyrroline, and 10 mM of NAD(P)H. After an incubation of 45 min at 25 °C, 3-methylpiperidine was added as internal standard, and the reaction was stopped with NaOH (final concentration 1.43 M). The samples were extracted with methyl *tert*-butyl ether (MTBE) and derivatized with acetic anhydride. Finally, the organic phases were analyzed by gas chromatography (GC) as described previously (Figures S7 and S8 in the Supporting Information).[37]

Acknowledgments

The research leading to these results has received support from the DFG (Deutsche Forschungsgemeinschaft). We want to thank Prof. Dr. Frances H. Arnold and Dr. Jackson K. B. Cahn for support regarding the usage of the CSR-SALAD tool.

Conflict of interest

The authors declare no conflict of interest.

Keywords: activity recovery · cofactor specificity · enzyme catalysis · imine reductase · site-directed mutagenesis

[1] M. Breuer, K. Ditrich, T. Habicher, B. Hauer, M. Keßeler, R. Stürmer, T. Zelinski, *Angew. Chem. Int. Ed.* **2004**, *43*, 788 – 824; *Angew. Chem.* **2004**, *116*, 806 – 843.
[2] R. C. Simon, B. Grischek, F. Zepeck, A. Steinreiber, F. Belaj, W. Kroutil, *Angew. Chem. Int. Ed.* **2012**, *51*, 6713 – 6716; *Angew. Chem.* **2012**, *124*, 6817 – 6820.
[3] M. T. Reetz, K. Schimossek, *Chimia* **1996**, *50*, 668 – 669.
[4] M. M. Heberling, B. Wu, S. Bartsch, D. B. Janssen, *Curr. Opin. Chem. Biol.* **2013**, *17*, 250 – 260.
[5] M. J. Abrahamson, E. Vázquez-Figueroa, N. B. Woodall, J. C. Moore, A. S. Bommarius, *Angew. Chem. Int. Ed.* **2012**, *51*, 3969 – 3972; *Angew. Chem.* **2012**, *124*, 4036 – 4040.
[6] E. O'Reilly, C. Iglesias, D. Ghislieri, J. Hopwood, J. L. Galman, R. C. Lloyd, N. J. Turner, *Angew. Chem. Int. Ed.* **2014**, *53*, 2447 – 2450; *Angew. Chem.* **2014**, *126*, 2479 – 2482.
[7] J. Mangas-Sanchez, S. P. France, S. L. Montgomery, G. A. Aleku, H. Man, M. Sharma, J. I. Ramsden, G. Grogan, N. J. Turner, *Curr. Opin. Chem. Biol.* **2017**, *37*, 19 – 25.
[8] P. N. Scheller, M. Lenz, S. C. Hammer, B. Hauer, B. M. Nestl, *ChemCatChem* **2015**, *7*, 3239 – 3242.
[9] H. Kohls, F. Steffen-Munsberg, M. Höhne, *Curr. Opin. Chem. Biol.* **2014**, *19*, 180 – 192.
[10] G. Grogan, N. J. Turner, *Chem. Eur. J.* **2016**, *22*, 1900 – 1907.
[11] P. Matzel, M. Gand, M. Höhne, *Green Chem.* **2017**, *19*, 385 – 389.
[12] S. P. France, S. Hussain, A. M. Hill, L. J. Hepworth, R. M. Howard, K. R. Mulholland, S. L. Flitsch, N. J. Turner, *ACS Catal.* **2016**, *6*, 3753 – 3759.
[13] F. Leipold, S. Hussain, D. Ghislieri, N. J. Turner, *ChemCatChem* **2013**, *5*, 3505 – 3508.
[14] Z. Maugeri, D. Rother, *J. Biotechnol.* **2017**, *258*, 167 – 170.
[15] W. A. van der Donk, H. Zhao, *Curr. Opin. Biotechnol.* **2003**, *14*, 421 – 426.
[16] R. Wichmann, D. Vasic-Racki, in *Technology Transfer in Biotechnology. Advances in Biochemical Engineering*, Vol. 92, (Ed.: U. Kragl), Springer, Berlin, **2005**, pp. 225 – 260.
[17] C. Rodriguez, I. Lavandera, V. Gotor, *Curr. Org. Chem.* **2012**, *16*, 2525 – 2541.
[18] W. Liu, P. Wang, *Biotechnol. Adv.* **2007**, *25*, 369 – 384.
[19] A. Weckbecker, W. Hummel, *Microb. Enzymes Biotransform.* **2005**, *17*, 225 – 238.
[20] C.-H. Wong, G. M. Whitesides, *J. Am. Chem. Soc.* **1981**, *103*, 4890 – 4899.
[21] A. S. Bommarius, K. Drauz, W. Hummel, M. R. Kula, C. Wandrey, *Biocatal. Biotransform.* **1994**, *10*, 37 – 47.
[22] Z. Shaked, G. M. Whitesides, *J. Am. Chem. Soc.* **1980**, *102*, 7104 – 7105.
[23] J. M. Vrtis, A. K. White, W. W. Metcalf, W. A. van der Donk, *Angew. Chem. Int. Ed.* **2002**, *41*, 3257 – 3259; *Angew. Chem.* **2002**, *114*, 3391 – 3393.
[24] J. Ratzka, L. Lauterbach, O. Lenz, M. B. Ansorge-Schumacher, *Biocatal. Biotransform.* **2011**, *29*, 246 – 252.
[25] L. Lauterbach, O. Lenz, K. A. Vincent, *FEBS J.* **2013**, *280*, 3058 – 3068.
[26] M. Rodríguez-Mata, A. Frank, E. Wells, F. Leipold, N. J. Turner, S. Hart, J. P. Turkenburg, G. Grogan, *ChemBioChem* **2013**, *14*, 1372 – 1379.
[27] K. Seelbach, B. Riebel, W. Hummel, M.-R. Kula, V. I. Tishkov, A. M. Egorov, C. Wandrey, U. Kragl, *Tetrahedron Lett.* **1996**, *37*, 1377 – 1380.
[28] V. I. Tishkov, V. O. Popov, *Biomol. Eng.* **2006**, *23*, 89 – 110.
[29] K. Hoelsch, I. Sührer, M. Heusel, D. Weuster-Botz, *Appl. Microbiol. Biotechnol.* **2013**, *97*, 2473 – 2481.
[30] R. Woodyer, W. A. van der Donk, H. Zhao, *Biochemistry* **2003**, *42*, 11604 – 11614.
[31] T. W. Johannes, R. D. Woodyer, H. Zhao, *Biotechnol. Bioeng.* **2007**, *96*, 18 – 26.
[32] R. A. Chica, N. Doucet, J. N. Pelletier, *Curr. Opin. Biotechnol.* **2005**, *16*, 378 – 384.
[33] K. A. Kretz, T. H. Richardson, K. A. Gray, D. E. Robertson, X. Tan, J. M. Short, *Methods Enzymol.* **2004**, *388*, 3 – 11.
[34] M. Gand, C. Thöle, H. Müller, H. Brundiek, G. Bashiri, M. Höhne, *J. Biotechnol.* **2016**, *230*, 11 – 18.
[35] J. K. B. Cahn, C. A. Werlang, A. Baumschlager, S. Brinkmann-Chen, S. L. Mayo, F. H. Arnold, *ACS Synth. Biol.* **2017**, *6*, 326 – 333.
[36] E. Krieger, G. Koraimann, G. Vriend, *Proteins Struct. Funct. Bioinf.* **2002**, *47*, 393 – 402.
[37] M. Lenz, J. Meisner, L. Quertinmont, S. Lutz, J. Kästner, B. M. Nestl, *ChemBioChem* **2017**, *18*, 253 – 256.

Manuscript received: July 21, 2017
Revised manuscript received: August 22, 2017
Accepted manuscript online: August 28, 2017
Version of record online: November 29, 2017